Chapter 4

A Model of an Experiment on Endothelial Cell Migration

In this chapter, the reinforced random walk theory described in chapter 3 will be used to formulate a mathematical model of EC migration. Specifically, we model the experimental setup of [169], in which an aggregate of EC was placed at the centre of a disc and exposed to varying concentrations of angiogenic factors. The object of this work is to develop the model for EC migration in close conjunction with empirical data. A realistic *in vivo* scenario of tumour angiogenesis will be modelled in subsequent chapters.

In section 4.1, the experimental setup is described in detail. In section 4.2, we build the mathematical model, which describes how the EC move and how the substrates evolve. In section 4.3, the method of simulation is described and in section 4.4, the model parameters are discussed. In section 4.5, the results are presented and compared with the experimental data and, finally, section 4.6 contains a discussion of the results.

4.1 The Experiment

The experiment of Vernon and Sage [169] investigates "radial invasion of matrix by aggregated cells" (RIMAC) in the presence of different growth factors. The assay consists of placing an aggregate of EC at the centre of a disc of collagen,

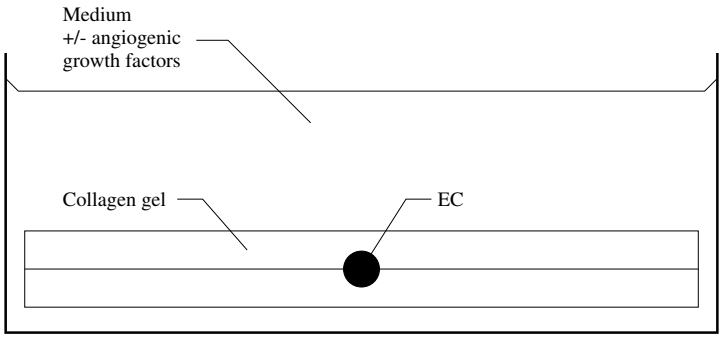

Figure 4.1: A diagram of the experiment.

immersed in medium +/− angiogenic growth factors. After five days, the EC are scored for radial invasion into the surrounding collagen gel. Figure 4.1 shows a diagram of the experimental setup. The growth factors tested, at varying levels and combinations, include VEGF, bFGF and TGF-β1. Here, we concentrate on VEGF, the best characterised EC-specific growth factor [55].

RIMAC is an experimental technique for assessing the response of cells to diffusing proteins in general. The aim of the experiment is to identify the effects of different angiogenic substances on EC migration, clearly an essential step towards understanding angiogenesis. We formulate a reinforced random walk type model, which forms the basis for simulations of the experiment. The aim is to develop a model, which, while being mathematically tractable, is directly derived from the underlying biology.

In the full three-dimensional model, we assume that the VEGF concentration is in steady state. However, we also formulate a two-dimensional model in which we relax this assumption and allow for diffusion and uptake of VEGF. We then consider the effect of placing a point source of VEGF on the edge of the disc, in order to investigate the directional response of the EC to a chemotactic gradient (see Figure 4.2).

4.2 The Mathematical Model

The model is constructed on a cylinder of radius R and height $2H$,

$$\Omega = \left\{(x, y, z) \in \mathbb{R}^3 : x^2 + y^2 \leq R^2,\ -H \leq z \leq H\right\}.$$

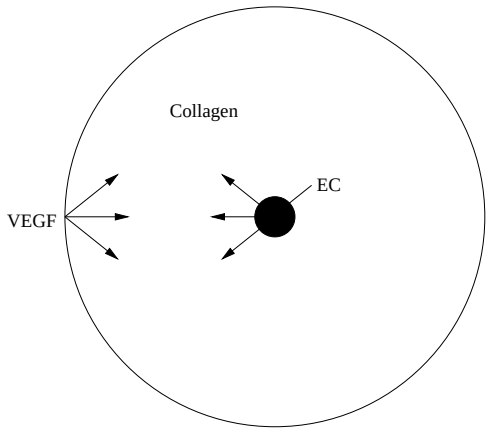

Figure 4.2: The two-dimensional model with a point source of VEGF.

Initially, collagen is distributed uniformly over the domain, representing the collagen gel. We neglect collagen diffusion since the rate of diffusion of large macromolecules is very low. EC are known to synthesise ECM components during sprout formation [35, 66], so we include deposition of collagen by EC.

VEGF is applied at a constant concentration on the boundary, and is then allowed to diffuse throughout the domain. A term is included modelling uptake and binding of VEGF by the EC. Upper and lower functions for the solution to the resulting reaction–diffusion equation for VEGF are obtained using comparison principles. Simulations are then run with the steady state solutions of both the upper and the lower functions.

The EC are initially arranged in a spherical aggregate (of radius $r_i < H < R$) at the centre of the domain. Each cell is subsequently permitted to move around on a regular finite grid, obeying the rules of a reinforced random walk. VEGF is viewed as a chemotactic and chemokinetic factor for EC [55, 77]. In other words, VEGF promotes both random migration and directed migration up a VEGF concentration gradient. Collagen is assumed to assist EC adhesion by haptotaxis [4, 21]. The random walk is therefore set up so that EC are attracted to areas of higher VEGF and higher collagen concentrations. The behaviour of the EC is then examined under various conditions, and the results compared to the experimental results of [169].

The three quantities of interest are EC density, $p\,(x, y, z, t)$, VEGF concentration, $v\,(x, y, z, t)$, and collagen concentration, $c\,(x, y, z, t)$, at (x, y, z) and time t.

4.2.1 The Endothelial Cell Dynamics

For clarity, the equations in this section will be presented in two dimensions, but readily generalise to the three-dimensional form used in the simulations. We assume that the EC move on a regular grid (of step size h) and denote the EC (probability) density at grid point (n, m) at time t by $p_{n,m}(t)$.

The EC are assumed to obey the master equation (3.10):

$$\begin{aligned}\frac{\partial p_{n,m}}{\partial t} &= \hat{\tau}^{H+}_{n-1,m}p_{n-1,m} + \hat{\tau}^{H-}_{n+1,m}p_{n+1,m} + \hat{\tau}^{V+}_{n,m-1}p_{n,m-1} + \hat{\tau}^{V-}_{n,m+1}p_{n,m+1} \\ &\quad - \left(\hat{\tau}^{H+}_{n,m} + \hat{\tau}^{H-}_{n,m} + \hat{\tau}^{V+}_{n,m} + \hat{\tau}^{V-}_{n,m}\right) p_{n,m}. \end{aligned} \tag{4.1}$$

In order to incorporate both chemotactic (gradient-driven) and chemokinetic (diffusion-driven) stimuli, we use a combination of the normalised and unnormalised barrier models of [117] for the transition rates, as described in section 3.4.2:

$$\begin{aligned}\hat{\tau}^{H\pm}_{n,m} &= \lambda\left(\frac{4\tau\left(w_{n\pm\frac{1}{2},m}\right)}{\tau\left(w_{n-\frac{1}{2},m}\right) + \tau\left(w_{n+\frac{1}{2},m}\right) + \tau\left(w_{n,m-\frac{1}{2}}\right) + \tau\left(w_{n,m+\frac{1}{2}}\right)}\right. \\ &\quad \left. + \frac{D\left(w_{n\pm\frac{1}{2},m}\right)}{D_0} - 1\right), \end{aligned} \tag{4.2}$$

$$\begin{aligned}\hat{\tau}^{V\pm}_{n,m} &= \lambda\left(\frac{4\tau\left(w_{n,m\pm\frac{1}{2}}\right)}{\tau\left(w_{n-\frac{1}{2},m}\right) + \tau\left(w_{n+\frac{1}{2},m}\right) + \tau\left(w_{n,m-\frac{1}{2}}\right) + \tau\left(w_{n,m+\frac{1}{2}}\right)}\right. \\ &\quad \left. + \frac{D\left(w_{n,m\pm\frac{1}{2}}\right)}{D_0} - 1\right), \end{aligned} \tag{4.3}$$

for some functions, $\tau(w)$ and $D(w)$, and constant, $D_0 > 0$. As already mentioned, the disadvantage of this method is the introduction of the arbitrary parameter, $D_0 > 0$, into the transition rates, to which the continuum limit PDE is invariant.

Various choices are possible for the function $\tau(w) \equiv \tau_1(v)\,\tau_2(c)$. For example, classical chemotaxis [107] would, by (3.40), lead to a transition probability function of the form $\tau_1(v) = \exp\left(\frac{\chi_0 v}{D_0}\right)$. We make the more realistic assumption that EC sensitivity is reduced in regions where the concentration of chemoattractant is high, reflecting saturation of the cell receptors. Following [4, 12], we use a receptor–kinetic law of the form

$$\chi(v) = \frac{\chi_0}{1 + \gamma_1 v}.$$

In the absence of evidence regarding functional forms, we assume a similar law for the haptotactic coefficient, $\rho(c)$. Hence, by (3.40),

$$\tau_1(v) = (1+\gamma_1 v)^{\frac{\chi_0}{\gamma_1 D_0}}, \quad \tau_2(c) = (1+\gamma_2 c)^{\frac{\rho_0}{\gamma_2 D_0}}, \tag{4.4}$$

where $\chi_0, \rho_0, \gamma_1, \gamma_2$ are constants.

The continuum limit of the master equation (4.1) is then:

$$\frac{\partial p}{\partial t} = \nabla.\left(D(v,c)\nabla p\right) - \nabla.\left(\frac{\chi_0}{1+\gamma_1 v} p \nabla v\right) - \nabla.\left(\frac{\rho_0}{1+\gamma_2 c} p \nabla c\right). \tag{4.5}$$

Since the EC are stimulated to move up VEGF gradients and up collagen gradients, we take $\chi_0, \rho_0 > 0$. We choose γ_1 to be of order $O\left(v^{-1}\right)$ and γ_2 to be $O\left(c^{-1}\right)$, so that desensitisation occurs at biologically realistic levels of v and c.

In addition to the directional response of the EC to VEGF and collagen, we include an increase in diffusive motility at higher VEGF concentrations. We wish $D(v)$ to be an increasing function of v, which varies between positive upper and lower bounds. We therefore take the rational form:

$$D(v) = D_m \frac{v+\theta_1}{v+\theta_2}, \tag{4.6}$$

for constants $D_m > 0$ and $0 < \theta_1 < \theta_2$. $D(0) = D_m \frac{\theta_1}{\theta_2}$, so there will still be some random motility in the absence of any VEGF. $D(v) \to D_m$ as $v \to \infty$, so the diffusion coefficient does not increase without bound as the VEGF concentration grows very large, but saturates to a limiting value.

Initially, there is an aggregate of EC (of radius r_i) centred on $(0,0,0)$, so we start by placing one EC at each grid point in $\left\{(x,y,z) \in \Omega : x^2+y^2+z^2 \le r_i^2\right\}$. The EC cannot move outside the disc, so we impose no flux of EC across the boundary $\partial\Omega$.

These conditions may be written (in continuum form) as

$$p(x,y,z,0) = \left\{ \begin{array}{ll} p_0, & x^2+y^2+z^2 \le r_i^2 \\ 0, & x^2+y^2+z^2 > r_i^2 \end{array} \right\}, \tag{4.7}$$

$$0 = D(v)\frac{\partial p}{\partial n} - D_0 \frac{p}{\tau}\frac{\partial \tau}{\partial n}, \qquad \text{on } \partial\Omega \times [0,T], \tag{4.8}$$

where $\frac{\partial}{\partial n}$ is the normal derivative on the boundary $\partial\Omega$.

4.2.2 The Substrate Dynamics

VEGF binds to receptors on the endothelial cell surface and this stimulates the EC to produce a proteolytic enzyme (or protease), capable of degrading extra-cellular proteins [121]. Here, we are not concerned with proteolysis, but we do incorporate uptake of VEGF by EC, which we assume occurs at constant rate, $\alpha \geq 0$. We include a natural, Fickian diffusion term (with diffusion coefficient, $D_v \geq 0$) to arrive at the governing equation for VEGF:

$$\frac{\partial v}{\partial t} = D_v \nabla^2 v - \alpha p v, \quad \text{on } \Omega \times [0, T]\,. \tag{4.9}$$

In the experiment [169], there is initially no VEGF in the domain, except on the boundary where it is at a uniform level, $v_0 > 0$. This gives the initial condition:

$$v\,(x, y, z, 0) = \left\{ \begin{array}{ll} 0 & \text{inside } \Omega \\ v_0 & \text{on } \partial\Omega \end{array} \right\}. \tag{4.10}$$

Furthermore, since the disc is suspended in a relatively large container of medium, the VEGF concentration on the boundary can be assumed to remain at this constant level throughout. We therefore have the Dirichlet boundary condition:

$$v\,(x, y, z, t) = v_0, \quad \text{on } \partial\Omega \times [0, T]\,. \tag{4.11}$$

In the experiment, the disc was initially covered with a collagen gel of uniform concentration. In addition to this initial level, we assume that the EC deposit collagen [66, 120], according to the logistic growth equation used by [87]:

$$\frac{\partial c}{\partial t} = \beta p c\,(C - c)\,, \quad \text{on } \Omega \times [0, T]\,, \tag{4.12}$$

where $\beta, C \geq 0$ are constants.

Thus the collagen concentration will increase in the presence of EC (when $p > 0$), but cannot rise above a fixed maximum concentration, C. Collagen is a large macromolecule, so its diffusion will take place very slowly. We therefore neglect collagen diffusion.

The collagen is initially of uniform concentration, $c_0 \in (0, C)$, giving the initial condition

$$c\,(x, y, z, 0) = c_0, \quad \text{on } \Omega. \tag{4.13}$$

4.2.3 Non-Dimensionalisation

Let

$$\begin{array}{llllll} p' = \frac{p}{p_0}, & v' = \frac{v}{V}, & c' = \frac{c}{C}, & x' = \frac{x}{R}, & y' = \frac{y}{R}, & z' = \frac{z}{R} \\ t' = \frac{t}{T}, & D'_m = \frac{D_m T}{R^2}, & D'_0 = \frac{D_0 T}{R^2}, & D'_v = \frac{D_v T}{R^2}, & \alpha' = T p_0 \alpha, & \beta' = T p_0 C \beta \\ \gamma'_1 = V\gamma_1, & \gamma'_2 = C\gamma_2, & v'_0 = \frac{v_0}{V}, & c'_0 = \frac{c_0}{C}, & \theta'_1 = \frac{\theta_1}{V}, & \theta'_2 = \frac{\theta_2}{V} \\ H' = \frac{H}{R}, & q_1 = \frac{\chi_0}{\gamma_1 D_0}, & q_2 = \frac{\rho_0}{\gamma_2 D_0}, & r'_i = \frac{r_i}{R}. & & \end{array}$$

The governing equations (4.1), (4.9), (4.12), on dropping the dashes, become

$$\begin{aligned} \frac{\partial p_{n,m}}{\partial t} &= \hat{\tau}^{H+}_{n-1,m} p_{n-1,m} + \hat{\tau}^{H-}_{n+1,m} p_{n+1,m} + \hat{\tau}^{V+}_{n,m-1} p_{n,m-1} + \hat{\tau}^{V-}_{n,m+1} p_{n,m+1} \\ &\quad - \left(\hat{\tau}^{H+}_{n,m} + \hat{\tau}^{H-}_{n,m} + \hat{\tau}^{V+}_{n,m} + \hat{\tau}^{V-}_{n,m}\right) p_{n,m}, \qquad (4.14) \\ \frac{\partial v}{\partial t} &= D_v \nabla^2 v - \alpha p v, \qquad (4.15) \\ \frac{\partial c}{\partial t} &= \beta p c \left(1 - c\right), \qquad (4.16) \end{aligned}$$

on $\Omega = \left\{(x, y, z) \in \mathbb{R}^3 : x^2 + y^2 \leq 1, -H \leq z \leq H\right\}$, $t \in [0, 1]$.

The transition rates (4.2)–(4.6) are given by

$$\begin{aligned} \hat{\tau}^{H\pm}_{n,m} &= \lambda \left(\frac{4\tau\left(w_{n\pm\frac{1}{2},m}\right)}{\tau\left(w_{n-\frac{1}{2},m}\right) + \tau\left(w_{n+\frac{1}{2},m}\right) + \tau\left(w_{n,m-\frac{1}{2}}\right) + \tau\left(w_{n,m+\frac{1}{2}}\right)} \right. \\ &\quad \left. + \frac{D\left(w_{n\pm\frac{1}{2},m}\right)}{D_0} - 1 \right), \qquad (4.17) \\ \hat{\tau}^{V\pm}_{n,m} &= \lambda \left(\frac{4\tau\left(w_{n,m\pm\frac{1}{2}}\right)}{\tau\left(w_{n-\frac{1}{2},m}\right) + \tau\left(w_{n+\frac{1}{2},m}\right) + \tau\left(w_{n,m-\frac{1}{2}}\right) + \tau\left(w_{n,m+\frac{1}{2}}\right)} \right. \\ &\quad \left. + \frac{D\left(w_{n,m\pm\frac{1}{2}}\right)}{D_0} - 1 \right), \qquad (4.18) \end{aligned}$$

where

$$\begin{aligned} \tau\left(v, c\right) &= \left(1 + \gamma_1 v\right)^{q_1} \left(1 + \gamma_2 c\right)^{q_2}, \qquad (4.19) \\ D\left(v\right) &= D_m \frac{v + \theta_1}{v + \theta_2}, \qquad (4.20) \\ \lambda &= \frac{D_0}{h^2}. \qquad (4.21) \end{aligned}$$

The initial conditions (4.7), (4.10), (4.13) and boundary conditions (4.8), (4.11) are

as follows.

$$\begin{array}{ll} \text{On } \Omega: & \text{On } \partial\Omega \times [0,1]: \end{array}$$

$$p(x,y,z,0) = \left\{ \begin{array}{ll} 1, & x^2+y^2+z^2 \leq r_i^2 \\ 0, & x^2+y^2+z^2 > r_i^2 \end{array} \right\}, \qquad \frac{D(v)}{D_0 p}\frac{\partial p}{\partial n} = \frac{1}{\tau}\frac{\partial \tau}{\partial n}, \tag{4.22}$$

$$v(x,y,z,0) = \left\{ \begin{array}{ll} 0 & \text{inside } \Omega \\ v_0 & \text{on } \partial\Omega \end{array} \right\}, \qquad v(x,y,z,t) = v_0, \tag{4.23}$$

$$c(x,y,z,0) = c_0. \tag{4.24}$$

In the three-dimensional simulations, we do not wish to solve the full reaction–diffusion equation for VEGF (4.15). We therefore construct lower and upper functions (v_1 and v_2 respectively) for the solution to this equation using comparison principles (see appendix B). The solution, v, of equation (4.15) thus satisfies

$$v_1(x,y,z,t) \leq v(x,y,z,t) \leq v_2(x,y,z,t), \quad \text{on } \Omega \times [0,1].$$

In the case of the lower function, v_1, the solution rapidly evolves to a steady state, $v_{1,s}$. For the upper function, v_2, evolution to the steady state, $v_{2,s}$ (which is spatially homogeneous), takes place more slowly. Nevertheless, $v_{2,s}$ is still an upper function for v, so we will use the steady states $v_{1,s}$ and $v_{2,s}$ in the simulations. The effects of using the time-dependent upper solution, which is intermediate between these two extremes and is likely to approximate the actual VEGF profile more closely, will also be discussed. The steady state solutions are given by:

$$\begin{aligned} v_{1,s}(x,y,z) &= v_0 \left(\frac{\cosh\left(\sqrt{\frac{\alpha}{D_v}}z\right)}{\cosh\left(\sqrt{\frac{\alpha}{D_v}}H\right)} \right. \\ &\quad \left. + \sum_{n=1}^{\infty} A_n I_0\left(\sqrt{\lambda_n (x^2+y^2)}\right) \cos\left((2n-1)\frac{\pi z}{2H}\right) \right), \end{aligned} \tag{4.25}$$

$$v_{2,s}(x,y,z) = v_0, \tag{4.26}$$

where

$$\lambda_n = \frac{\alpha}{D_v} + \frac{\pi^2 (2n-1)^2}{4H^2},$$

and the A_n are Fourier coefficients. One set of simulations is run with $v = v_{1,s}$ and one set with $v = v_{2,s}$.

We subsequently run two-dimensional simulations, on $\bar{\Omega} = \left\{(x,y) \in \mathbb{R}^2 : x^2+y^2 \leq 1\right\}$ with the full VEGF dynamics (4.15). However, in order to isolate the directional

response of the EC, we modify the initial and boundary conditions for VEGF to represent a point source at $(x, y) = (-1, 0)$, as opposed to a uniform source on $\partial\bar{\Omega}$. We therefore use the conditions

$$v(x, y, z, 0) = \left\{ \begin{array}{ll} 0 & \text{inside } \bar{\Omega} \\ v_0 \exp\left(-K\left((x+1)^2 + y^2\right)\right) & \text{on } \partial\bar{\Omega} \end{array} \right\}, \quad (4.27)$$

$$v(x, y, z, t) = v_0 \exp\left(-K\left((x+1)^2 + y^2\right)\right), \text{ on } \partial\bar{\Omega} \times [0, 1]. \quad (4.28)$$

4.3 The Method of Simulation

EC movement, governed by the master equation (4.14), is simulated as described in section 3.6. The method for three-dimensional simulations is very similar to that for two-dimensional simulations: a third set of transition rates, for movement in the z-direction, is defined analogously to (4.17) and (4.18). Note that if a cell ever reaches a mesh point adjacent to the boundary of the domain, it plays no further part in the simulation.

In the two-dimensional simulations, the VEGF values are updated at each time step according to (4.15), using a Crank–Nicolson numerical method (see appendix A).

The equation for collagen (4.16) may be solved to give

$$c(x, y, z, t + k) = \left[1 + \left(\frac{1}{c(x, y, z, t)} - 1\right) \exp\left(-\beta \int_t^{t+k} p(x, y, z, s)\, ds\right)\right]^{-1},$$

which is used to update the collagen values at each time step.

Note that the control substances are computed on an embedded lattice that is twice as fine as the lattice for cell movement. When updating values at a control substance node that is also on the cell movement lattice, $p(x, y, z, t)$ is taken to be 1 if the point (x, y, z) is occupied at time t and 0 if it is empty. At nodes that are not on the cell movement lattice, $p(x, y, z, t)$ is taken to be an average of the values at the adjacent points on the cell movement lattice.

At the end of the simulation, the cells are scored for radial invasion in the same way as in [169]. The disc is divided into 64 equal segments and the maximum radial invasion distance (regardless of the distance travelled in the z-direction) in each

Dimensional values	
Length of time of experiment	$T = 120$ h
Radius of disc	$R = 1.4$ mm
Half-height of disc	$H = 0.7$ mm
Radius of EC aggregate	$r_i = 0.134$ mm
Maximum EC diffusion coefficient	$D_m = 3.6 \times 10^{-4}$ mm^2/h
EC diffusion coefficient parameters	$\theta_1 = 2.5 \times 10^{-4}$ μg/ml
	$\theta_2 = 2.5 \times 10^{-3}$ μg/ml
VEGF diffusion coefficient	$D_v = 3.6 \times 10^{-3}$ mm^2/h
Chemotactic coefficient	$\chi_0 = 5.67$ mm^{2}h^{-1}ml μg^{-1}
Haptotactic coefficient	$\rho_0 = 7.88 \times 10^{-7}$ mm^{2}h^{-1}ml μg^{-1}
EC density in initial aggregate	$p_0 = 4444$ mm^{-2}
Boundary VEGF concentration	$V = v_0 = 5 \times 10^{-3}$ μg/ml
Initial collagen concentration	$c_0 = 600$ μg/ml
Maximum collagen concentration	$C = 2400$ μg/ml
VEGF uptake rate	$\alpha = 8.66 \times 10^{-5}$ mm^2/h
Collagen production coefficient	$\beta = 1.72 \times 10^{-9}$ mm^{2}h^{-1}ml μg^{-1}
Saturating parameter for VEGF	$\gamma_1 = 2000$ ml/μg
Saturating parameter for collagen	$\gamma_2 = 8.34 \times 10^{-4}$ ml/μg
Grid size	$h = 1.50 \times 10^{-2}$ mm
Time step size	$k = 0.12$ h
Dimensionless values	
Half-height of disc	$H = 0.5$
Maximum EC diffusion coefficient	$D_m = 0.0220$
EC diffusion coefficient parameters	$\theta_1 = 0.05$
	$\theta_2 = 0.5$
VEGF diffusion coefficient	$D_v = 0.220$
Exponent in VEGF TPF	$q_1 = \frac{\chi_0}{\gamma_1 D_p} = 78.8$
Exponent in collagen TPF	$q_2 = \frac{\rho_0}{\gamma_2 D_p} = 26.3$
Boundary VEGF concentration	$v_0 = 1$
Initial collagen concentration	$c_0 = 0.25$
VEGF uptake coefficient	$\alpha = 46.2$
Collagen production coefficient	$\beta = 2.20$
Radius of EC aggregate	$r_i = 9.59 \times 10^{-2}$
Saturation parameter for VEGF	$\gamma_1 = 10$
Saturation parameter for collagen	$\gamma_2 = 2$
Grid size	$h = 1.08 \times 10^{-2}$
Time step size	$k = 1 \times 10^{-3}$

Table 4.1: Parameter values used in the simulations.
TPF: transition probability function.

segment is noted. The average of these 64 values is then used as the radial invasion number.

4.4 Parameter Values

The parameter values used in the simulations are, unless otherwise stated, as shown in Table 4.1.

Diffusion coefficients. In [146], the range 2.48×10^{-5} mm^2/h – 1.26×10^{-4} mm^2/h was used for the epidermal cell diffusion coefficient. Here we choose D_m, θ_1, θ_2 so that the diffusion coefficient is $D = 3.6 \times 10^{-5}$ mm^2/h for $v = 0$, and that $D \to 3.6 \times 10^{-4}$ mm^2/h as $v \to \infty$. In [87], the diffusion coefficient for VEGF was taken to be $D_v = 3.6 \times 10^{-3}$ mm^2/h.

Time and length scales. The length of the experiment [169] was $T = 5$ days $= 120$ h. The radius of the disc aperture (small assay) was $R = 1.4$ mm and its height was $2H = 1.4$ mm.

Grid size. EC are assumed to be incompressible cubes of side-length 0.015 mm, taken as an average value from [3]. We therefore used a grid step size of 0.015 mm.

Size of EC aggregate. The aggregate used in [169] consisted of between 1000 and 5000 cells, arranged in a sphere of radius r_i. Taking an average value of 3000 cells and assuming the cells are packed at maximum density, we have $\frac{4\pi r_i^3}{3} = 3000\,(0.015 \text{ mm})^3$, so $r_i = 0.134$ mm.

VEGF and collagen levels. The standard level of VEGF applied was $v_0 = 5 \times 10^{-3}$ μg/ml. The initial collagen concentration was given as $c_0 = 600$ μg/ml. We assume that the collagen concentration cannot increase by a factor of more than 4, and hence take the maximum collagen level as $C = 2400$ μg/ml.

Reaction rates. The reaction rates, α and β, are difficult to specify accurately. We therefore take estimates based on reaction times as follows. If EC density is constant, the spatially uniform solution of the governing VEGF equation (4.9) can be written $v\,(t) = v_0 e^{-\alpha p t}$. Hence $\alpha = \frac{\ln 2}{p_0 T_h}$ where T_h is the half-life of VEGF at EC density, $p = p_0$. Half-lives for such reactions tend to be measured in hours [87] and we assume this reaction is quite fast relative to the length of the experiment. We

therefore estimate the half-life to be $T_h = 1.8$ h, which gives $\alpha = 8.66 \times 10^{-5}$ mm^2/h.

Similarly, for p constant, the solution to the governing collagen equation (4.12) can be written $c(t) = \frac{C}{\left(\frac{C}{c_0}-1\right)e^{-\beta C p t}+1}$. Clearly this tends to the maximum value, $C = 4c_0$, for large t, but let us make the assumption that, at EC density $p = p_0$, the collagen concentration will triple over the course of the experiment, i.e. $c(T) = 3c_0$. This gives $\beta = \frac{\ln 9}{C p_0 T} = 1.72 \times 10^{-9}$ mm^{2}h^{-1}mlμg^{-1}.

Chemotactic coefficient. A chemotactic coefficient of 9.36×10^8 mm^{2}h^{-1}M^{-1} was cited in [4]. The molecular weight of VEGF was taken by [87] to be 1.65×10^5 Da, so 1 M is equivalent to 1.65×10^8 μg/ml. Converting the above value into these units gives a chemotactic coefficient of $\chi_0 = 5.67$ mm^{2}h^{-1}mlμg^{-1}.

Haptotactic coefficient. The value of the haptotactic coefficient, ρ_0, is unknown. We assume that VEGF is a stronger attractant than collagen, and therefore choose ρ_0 such that the haptotactic exponent, q_2, is one third of the chemotactic exponent, q_1, in (4.19).

4.5 Results

Simulations of the system (4.14), (4.16)–(4.24) were run in three dimensions, firstly with VEGF concentration given by (4.26), and secondly by (4.25). Various boundary values for the VEGF concentration, v_0, were used.

Figure 4.3(a) shows a graph of radial invasion (as defined in section 4.3) against v_0, using the upper solution (4.26). As one would expect, increasing the VEGF level increases the invasive capacity of the cells; moreover, the graph exhibits good agreement with the experimental results shown in Figure 4.3(b). Since the VEGF concentration (4.26) is spatially uniform, there is no chemotaxis (gradient-driven migration) and the stimulus is entirely chemokinetic (diffusion-driven migration).

Figure 4.4 shows a plan view of the EC (i.e. their positions in the xy-plane) at $t = 0.0$, $t = 0.2$, $t = 0.4$, $t = 0.6$, $t = 0.8$ and $t = 1.0$ in a simulation using the upper solution for VEGF (4.26) and $v_0 = 1$. As expected, the cells gradually invade the surrounding matrix over time. Comparing the final positions of the EC in Figure 4.4 with experimental results (Figure 4.7(a)) shows that they are qualitatively

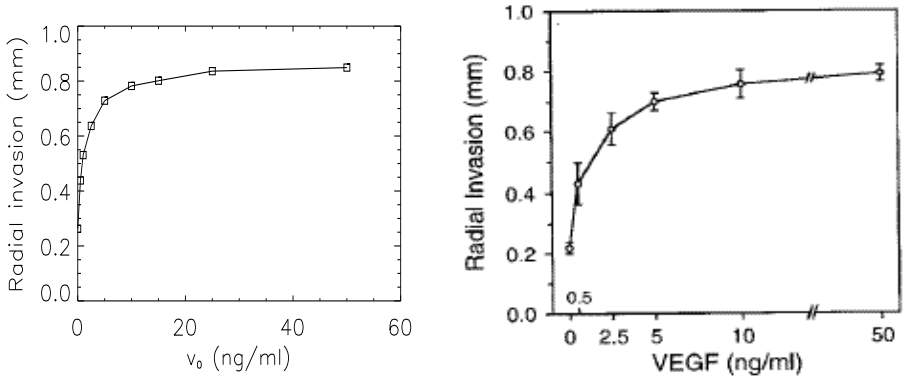

(a) (b)

Figure 4.3: A graph of average radial invasion against v_0, the VEGF concentration on the edge of this disc: (a) model predictions using the upper solution for VEGF (4.26). (b) experimental results of [169].

similar: the cells form outward trails from the initial aggregate in response to the chemokinetic effects of VEGF. Figure 4.5 shows the positions of the same cells in the xz-plane, illustrating the migration in the vertical (z) direction. Note that several cells have reached the upper and lower boundaries of the disc ($z = \pm 0.5$), and can subsequently move no further.

Figure 4.6 shows how the collagen profile develops; the concentration is plotted for $-H \leq z \leq H$ along the radial line $-1 \leq x \leq 1$, $y = 0$[1]. Since collagen diffusion is neglected in the model, the collagen level can only rise above its initial value where an EC is present. Unsurprisingly, it is in the centre of the domain, where the main body of cells is concentrated, that the collagen levels increase most rapidly. As time progresses, collagen is also laid down in areas away from the centre by invading cells. Although the profiles are rather erratic, it is clear that, at a given point in time, the general trend is for the collagen levels to decrease as one moves away from the centre. Thus, broadly speaking, haptotaxis will have the effect of holding the cells back.

It is possible that a number of cells are able to escape from the initial aggregate and subsequently move some distance into the matrix. As time passes, however, it becomes increasingly difficult to break away from the main cluster of cells due to

[1]Because of its dependence on the positions of the EC, which move stochastically, the collagen profile will not be exactly radially symmetrical, but the radial line plotted is representative.

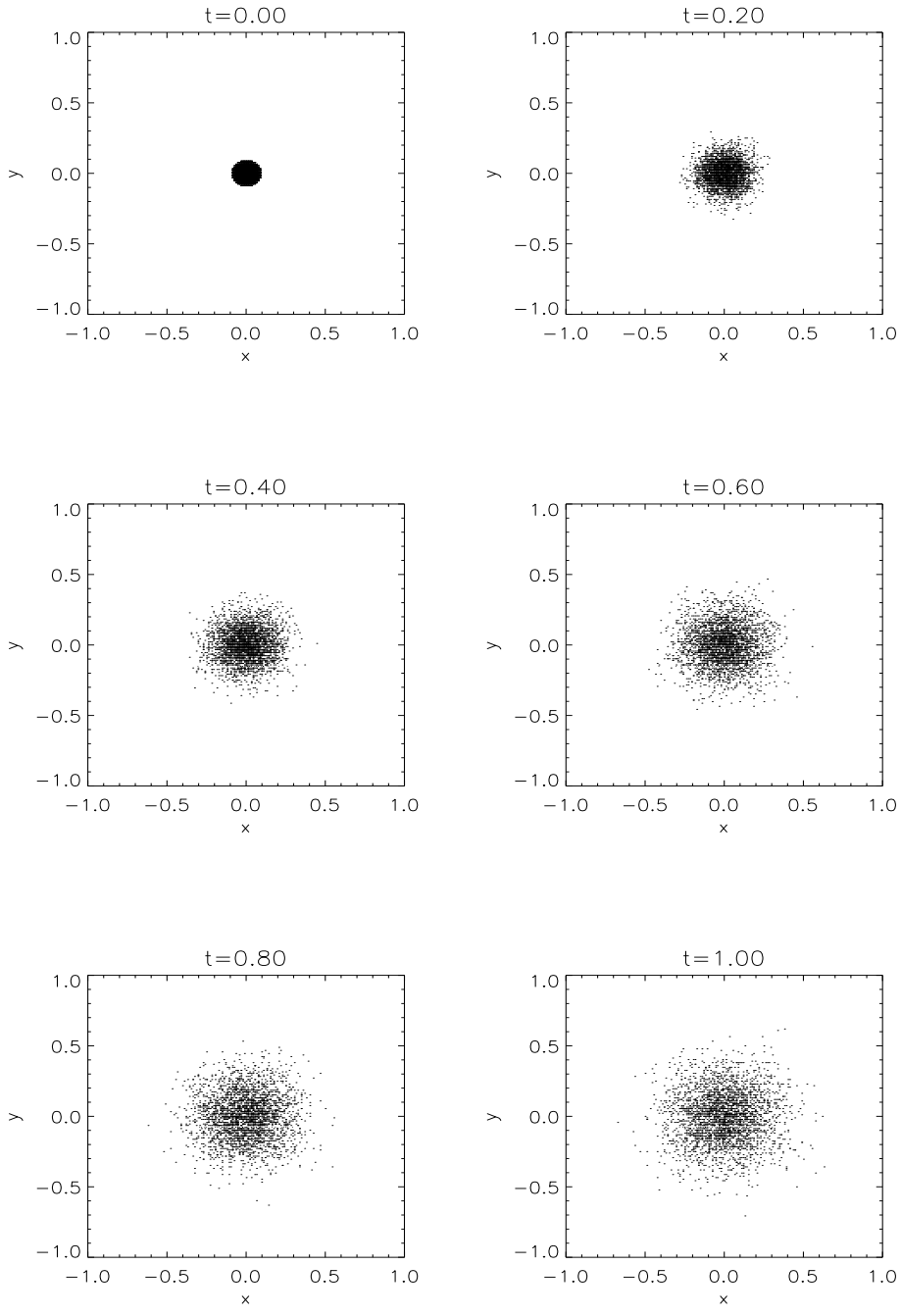

Figure 4.4: EC migration in the xy-plane in a simulation with the upper solution for VEGF (4.26) and $v_0 = 1$.

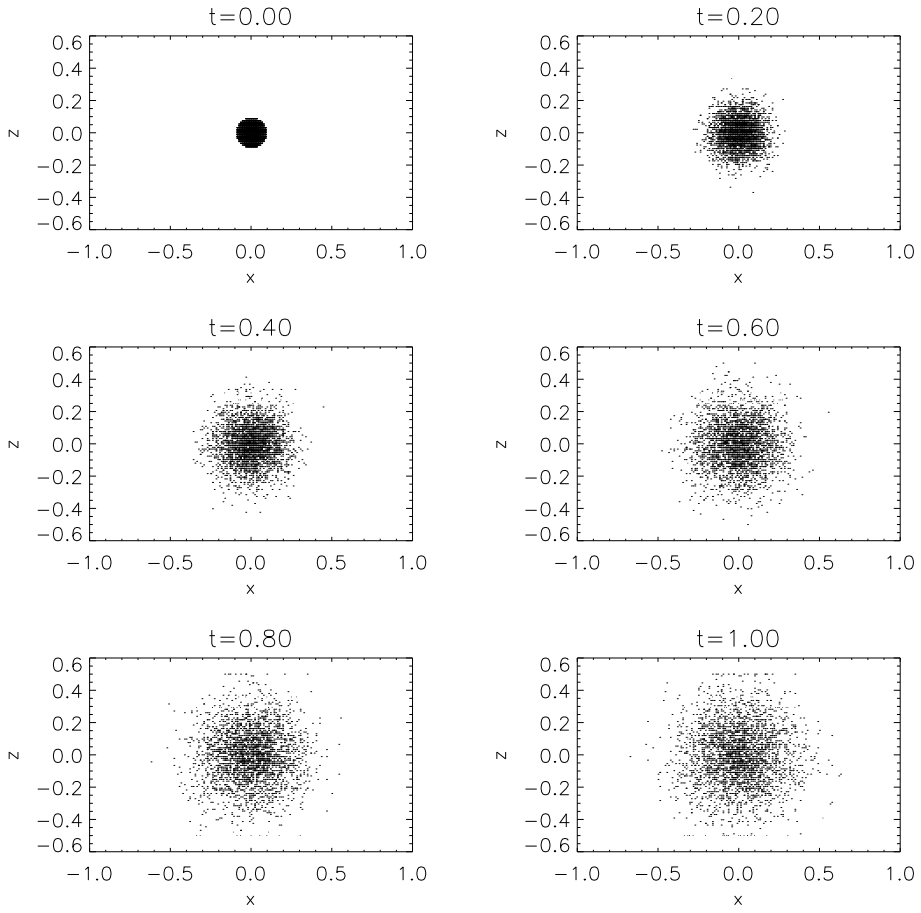

Figure 4.5: EC migration in the xz-plane in a simulation with the upper solution for VEGF (4.26) and $v_0 = 1$.

the strong inward pull of haptotaxis.

Figure 4.8 shows a simulation with $v_0 = 0.2$ (i.e. VEGF at one fifth of the standard concentration). Compared with Figure 4.4, the radial distances travelled by the EC into the matrix are significantly less. This reduced invasive capacity is due to the reduced diffusion coefficient of the EC (4.20). Similar results were observed by [169] at half the standard VEGF concentration: Figure 4.7(b) shows fewer invading cells and smaller invasion distances than Figure 4.7(a).

Figure 4.9 shows a simulation with no VEGF. Very few EC manage to break away from the initial aggregate and these do not move very far into the matrix. Again, the corresponding result of [169], Figure 4.7(c), shows good agreement, with very few cells moving very small distances.

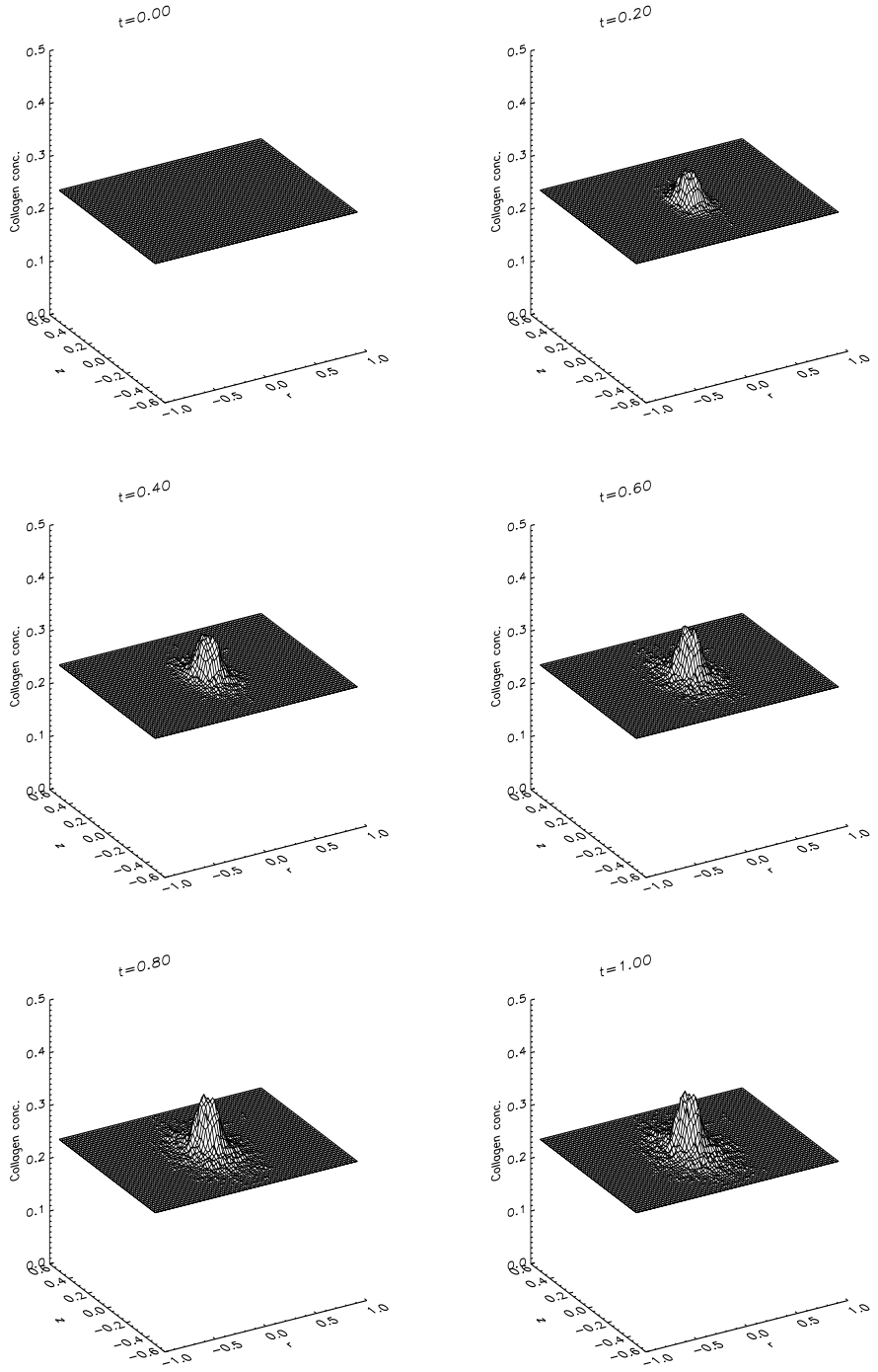

Figure 4.6: Evolution of the collagen profile in a simulation with the upper solution for VEGF (4.26) and $v_0 = 1$.

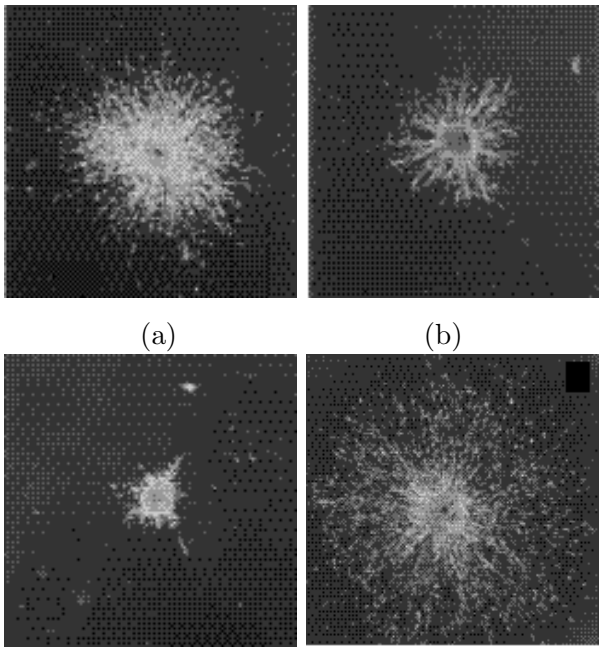

Figure 4.7: Experimental results of [169]: (a) VEGF concentration 5.0 ng/ml; collagen concentration 0.6 mg/ml; culture time 5 days. (b) Reduced VEGF concentration of 2.5 ng/ml; culture time 5 days. (c) No VEGF; culture time 5 days. (d) Very low collagen concentration; culture time 2 days.

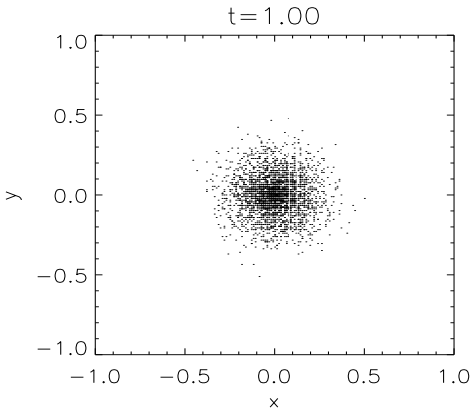

Figure 4.8: Positions of the EC after a simulation with the upper solution for VEGF (4.26) and $v_0 = 0.2$.

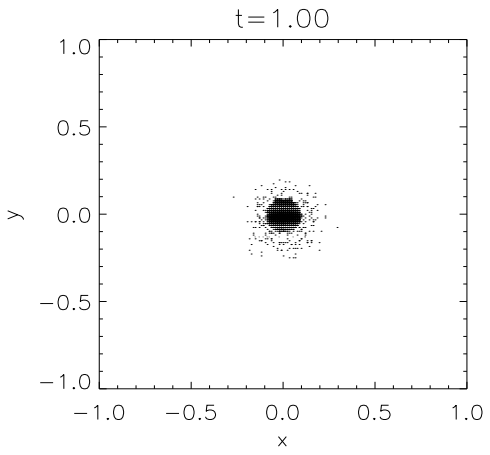

Figure 4.9: Positions of the EC after a simulation with $v_0 = 0$.

Figure 4.10 shows the results of a simulation using the *lower* solution for VEGF (4.25). The VEGF profile (Figure 4.10(c)) is no longer spatially uniform, but decreases as one moves towards the centre of the disc. There is therefore now a chemotactic stimulus for the EC to move up the VEGF concentration gradient, towards the boundary of the disc, in addition to the chemokinetic effects. Somewhat surprisingly, the radial invasion distances are significantly less than in the spatially uniform case (see Figure 4.4). However, the vertical migration distances are greater, with a large number of EC accumulating on the upper and lower surfaces of the disc. The reason for this is that the radius of the cylindrical domain, R, is greater than its height, H, so the distance between the initial aggregate and the upper and lower boundaries is less than the distance to the outer boundary. The VEGF gradient is steeper nearer to the boundary, $\partial\Omega$, so the EC are exposed to a greater chemotactic gradient in the z direction than in the x and y directions. Hence in this case chemotaxis favours vertical, as opposed to radial, migration.

It is difficult to compare this to the experimental results of [169] because they only examined radial migration. In addition, it is likely that the collagen matrix has a degree of anisotropy that introduces a bias (which is not accounted for in the mathematical model) for the cells to move predominantly in the equatorial plane ($z = 0$)[2].

[2]Phase-contrast microscopy shows that some of the collagen fibrils surrounding the EC aggregate in the RIMAC assay become radially aligned as a result of cellular traction. This is most likely a consequence of the supportive nylon mesh ring, which occupies the equatorial plane of the collagen matrix [168]. The radially aligned fibrils would offer less resistance to radial migration than to migration in the vertical direction [42].

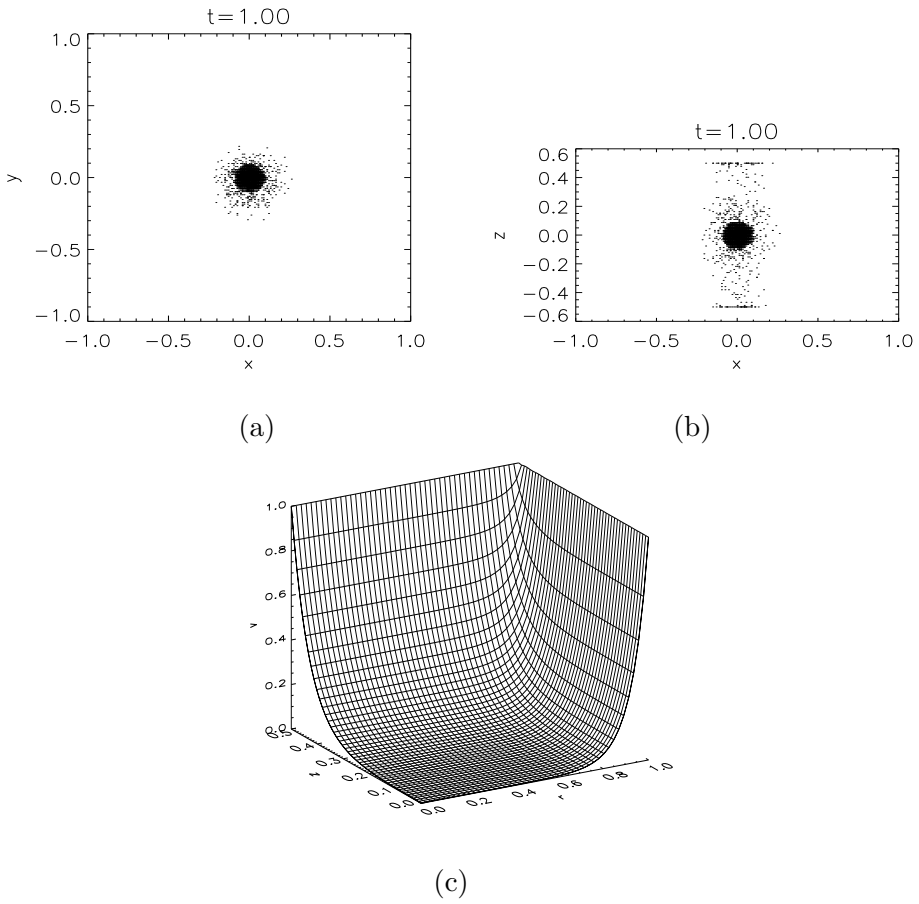

Figure 4.10: A simulation with the lower solution for VEGF (4.25) and $v_0 = 1$: (a) positions of the EC in the xy-plane. (b) positions of the EC in the xz-plane. (c) a graph of VEGF concentration against r and z.

The two sets of simulations correspond to two extreme cases of the VEGF profile. The lower solution effectively corresponds to the case where VEGF uptake occurs throughout the matrix, whereas in reality uptake would only occur where EC are present. The upper solution corresponds to no uptake, and the VEGF profile is spatially uniform. To gain some insight into the possible intermediate behaviour, we also ran simulations with the full time-dependent upper solution (see appendix A). The results are shown in Figure 4.11; the evolution of the VEGF profile may be seen in Figure 4.12. Radial migration is less pronounced than with the steady state upper solution (Figure 4.4), but more pronounced than with the lower solution (Figure 4.10(a)). Conversely, vertical migration is greater than with the steady state

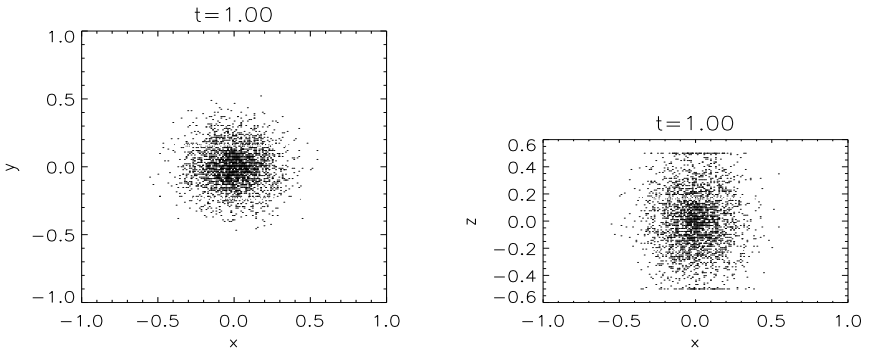

(a) (b)

Figure 4.11: A simulation with the full time-dependent upper solution for VEGF and $v_0 = 1$: (a) positions of the EC in the xy-plane. (b) positions of the EC in the xz-plane.

upper solution (Figure 4.5), but less than with the lower solution (Figure 4.10(b)). This is unsurprising since, in the simulation using the time-dependent solution, there are both chemotactic and chemokinetic stimuli: chemotaxis is the dominant effect at the beginning of the simulation, when the VEGF concentration is low, but the concentration gradients are large; chemokinesis dominates towards the end of the simulation, when the gradients have been largely destroyed by diffusion, but the concentration has risen almost to v_0. In contrast, the lower solution is dominated primarily by chemotaxis, whilst the steady-state upper solution provides only a chemokinetic stimulus.

Recall from section 4.2.1 that we introduced a parameter, D_0, to which the continuum limit equation (4.5) is invariant, but which does affect the transition probabilities (4.17)–(4.21). In the simulations, we took D_0 to be the minimum value of $D(v)$, thus ensuring that $\frac{D(v)}{D_0} - 1 \geq 0$, so the transition probabilities are always non-negative. This is the natural value to use, since the continuum limit of the master equation (3.38) decomposes into a taxis-containing term, with constant diffusion coefficient, D_0, and a random diffusive term, whose diffusion coefficient is the *excess* of $D(v)$ above D_0. Nevertheless, other choices, $D_0 < \min_{v \geq 0} D(v)$ are possible and it appears that reducing D_0 tends to reduce EC migration. This is a consequence of the finite grid size, h, and the dependence on D_0 vanishes in the limit $h \to 0$.

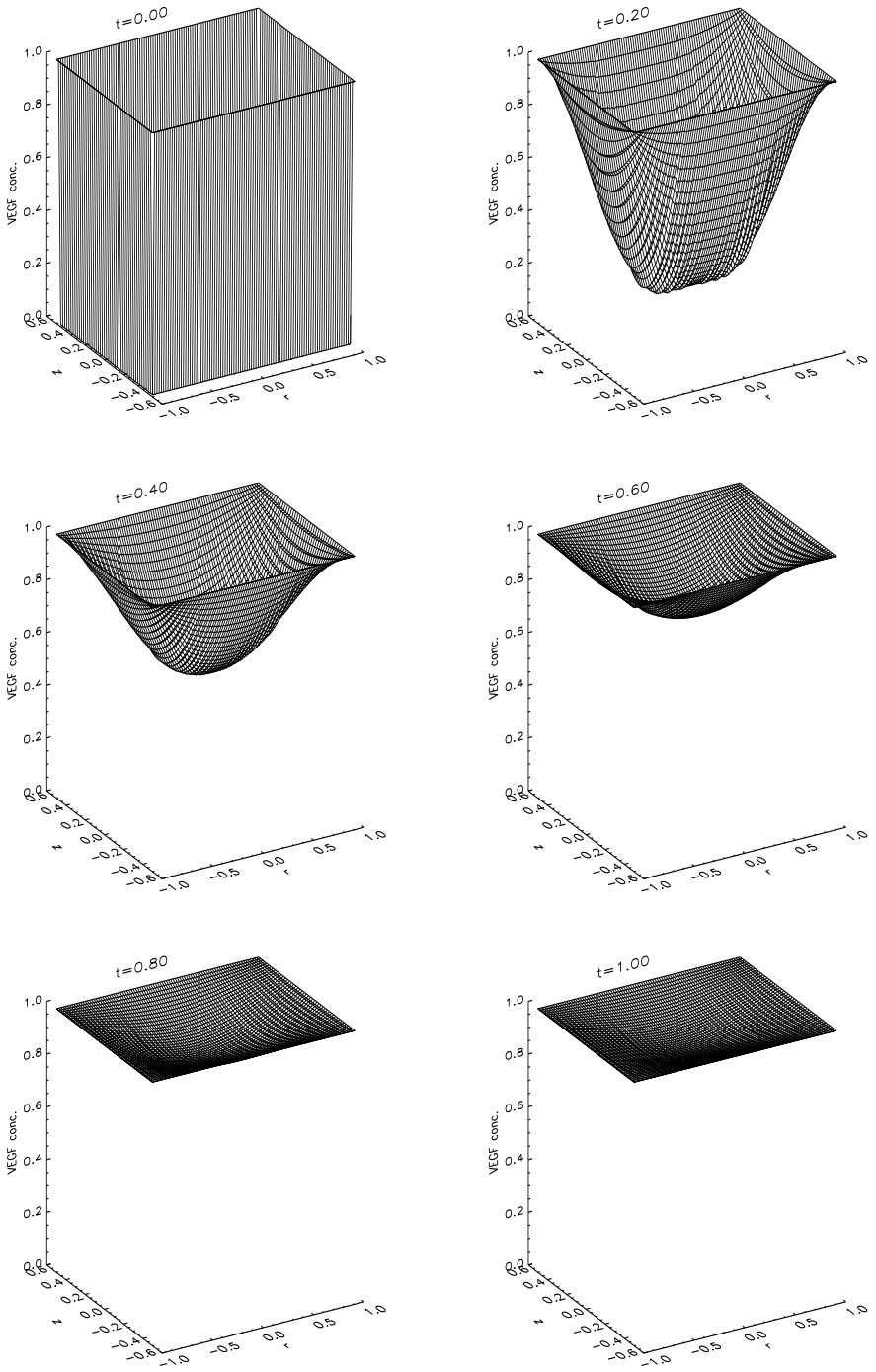

Figure 4.12: The time-dependent upper solution for VEGF.

We now turn to the two-dimensional simulations of the system (4.14)–(4.22), (4.24), (4.27), (4.28). These include the full VEGF dynamics (4.15), with a point source of VEGF on the edge of the disc at $(x, y) = (-1, 0)$. The VEGF diffuses into the disc and establishes a chemotactic gradient, stimulating the EC to move towards $(-1, 0)$. The effects of chemokinesis are still present, so diffusive motion will be greater at higher VEGF concentrations. However, the introduction of a point source of VEGF should make the *directional* response of the EC, via chemotaxis, more apparent.

Figure 4.13 shows the results of a simulation with $v_0 = 1$[3]. The migration is clearly biased to the left as the EC move up the VEGF concentration gradient shown in Figure 4.13(b); there is very little migration to the right.

As in the three-dimensional simulations, the collagen concentration is highest in the area corresponding to the initial EC aggregate. Thus haptotaxis will tend to hold the EC back (in contrast to chemotaxis, driving them towards the edge of the disc) and will therefore help to maintain the integrity of the central mass, which is still clearly visible at the end of the simulation. Note also that 'cords' of raised collagen concentration appear to grow out of the central mass. These cords presumably mark the path of one or more EC, as they leave a trail of increased collagen in their wake. It is possible that, once established by leading cells, these cords act as preferred paths for following EC, because of the cells' affinity for collagen. This is a similar scenario to the slime-following myxobacteria model of [117].

Removing the VEGF source removes both the directional and the random diffusive stimuli and, unsurprisingly, there is very little migration (results not shown). Conversely, increasing the boundary concentration of VEGF ($v_0 = 2$, Figure 4.14) increases the migration stimuli, resulting in greater invasion distances towards the point $(-1, 0)$.

Removing the collagen (Figure 4.15) removes haptotaxis and, in agreement with the hypothesis that haptotaxis helps to preserve the integrity of the initial aggregate, this results in the complete disintegration of the central mass of EC. This hypothesis is also borne out by the experimental results in Figure 4.7(d), in which the collagen matrix is at a greatly reduced concentration. After just 2 days, the distances travelled are clearly larger than in Figure 4.7(a), with some loss of cell–cell adhesion. This may be partly due to the fact that it is more difficult for EC to penetrate denser

[3]Note that, because we are effectively considering a two-dimensional cross-section through the full model, there are far fewer EC in the simulation.

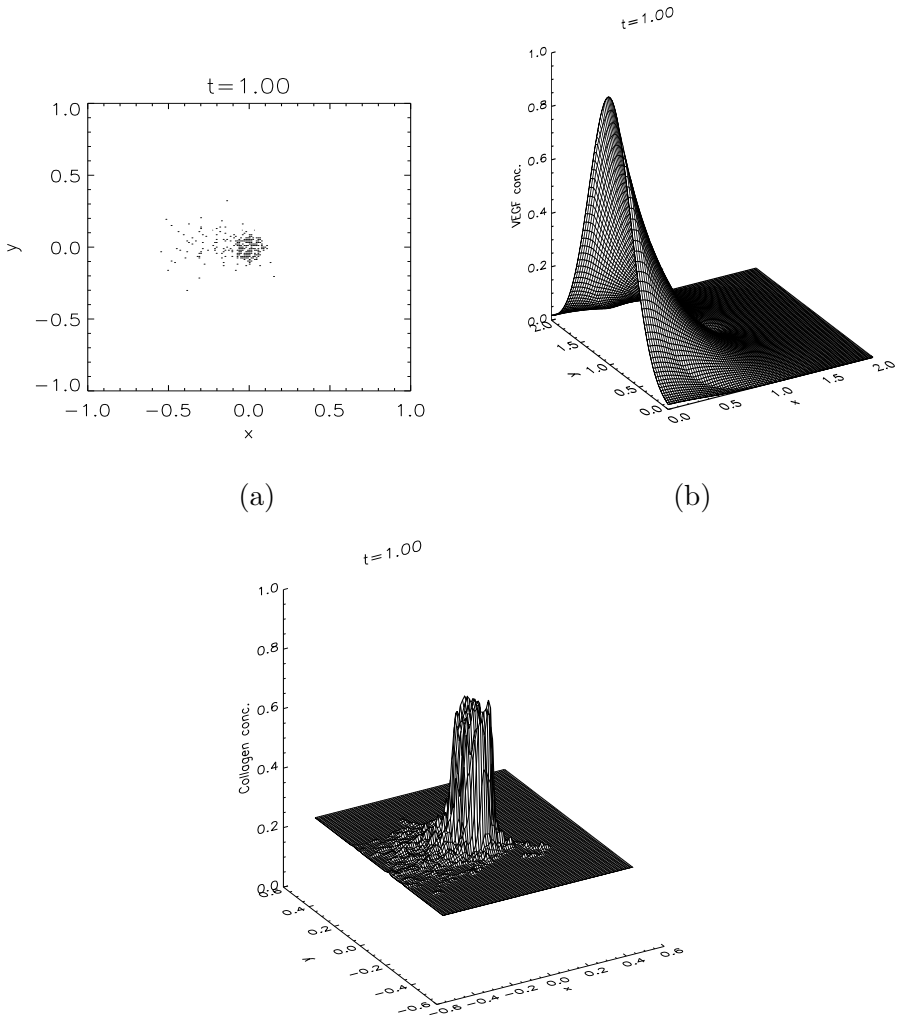

(a) (b)

(c)

Figure 4.13: A two-dimensional simulation with a point source of VEGF at $(-1, 0)$ and $v_0 = 1$: (a) positions of the EC. (b) VEGF concentration. (c) Collagen concentration.

collagen gels, so reducing the matrix density facilitates invasion. Nevertheless, it was observed that the low collagen concentration used in Figure 4.7(d) disrupted sprout branching and network formation.

4.6 Discussion

The basic model has demonstrated good qualitative agreement with *in vitro* experimental results. Nevertheless, there are many other considerations to be taken into account in a full model of angiogenesis. Clearly, the role of ECM components, such as collagen, in angiogenesis is highly complex and far from fully understood. To assume that haptotaxis acts by stimulating EC to migrate up a collagen concentration gradient is a massive simplification. For example, there may be concentration-dependent effects of ECM components on EC random motility; this could be included in our model in a similar way to the chemokinetic effects of VEGF. Also, during angiogenesis *in vivo*, degradation of the ECM by EC-derived proteolytic enzymes is an important step, facilitating matrix invasion [122]. This has been included in several models, both continuous [87] and discrete [4].

In this model, EC proliferation has been ignored but, during tumour angiogenesis, is a prerequisite for vascularisation (although initial sprouting can occur by EC migration alone) [148]. In the experiment, no proliferation was observed at low VEGF concentration; significant proliferation was observed at high VEGF concentration, although this was not crucial for matrix invasion [169]. Including proliferation into this model would enlarge the invading EC population, but the mechanism one should use for proliferation in an individual cell-based model is not obvious. The simplest way would be to assume, for each cell, a constant probability of mitotic division per unit time [151]. A more realistic way would be to use an increasing function of VEGF concentration for the proliferation probability, since VEGF is known to be a mitogen for EC [77]. The processes of EC proliferation and vessel branching and looping will be addressed in the following chapters.

In the experiment [169], the disc was immersed in medium, allowing growth factors to enter the collagen matrix from all sides. The symmetry of the setup thus made it difficult to distinguish between a chemokinetic response, in which EC movement is purely random, and a chemotactic response, in which EC movement is directed up a concentration gradient. It is likely that a combination of these two effects is

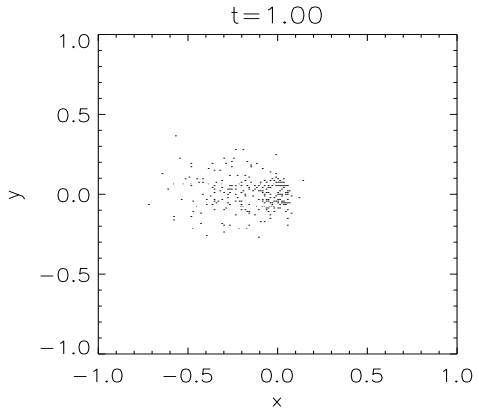

Figure 4.14: Positions of the EC after a two-dimensional simulation with a point source of VEGF at $(-1, 0)$ and $v_0 = 2$.

at work, but the experiment can shed no light on their relative contributions to the overall migratory response. For this reason, we constructed a two-dimensional model of a hypothetical experiment, with a point source of VEGF on the edge of the disc. This enabled us to isolate and investigate the directional response of the EC to a diffusible angiogenic factor, which is a crucial component of tumour angiogenesis. It would be interesting to compare the predictions of this model to data from an *in vitro* experiment of this nature. This would allow the model to be refined, in close conjunction with empirical data, helping to determine accurate functional forms for the transition probability function and the EC diffusion coefficient. The relative importance of chemokinesis and chemotaxis in EC migration could thereby be elucidated.

4.7 Summary

- The experimental setup of [169] has been modelled mathematically using reinforced random walks.
- The three-dimensional results, using analytic upper and lower solutions for VEGF, show good agreement with experimental data.
- The two-dimensional simulations (which include the reaction–diffusion equa-

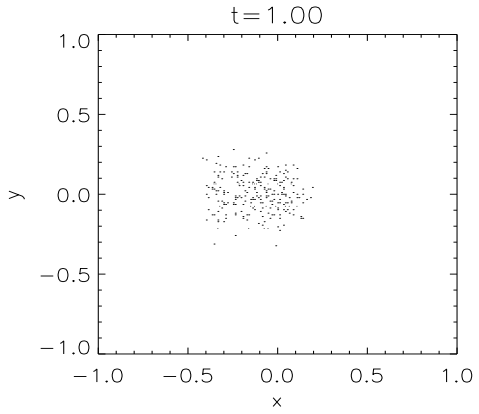

Figure 4.15: Positions of the EC after a two-dimensional simulation with a point source of VEGF at $(-1, 0)$, $v_0 = 1$ and no collagen.

tion for VEGF) of a hypothetical experiment enable the directional response of the EC, a crucial component of angiogenesis, to be observed independently of the diffusive response.

- Key references: Vernon and Sage [169], Plank *et al.* [127].